Control Strategy for a Droop-Controlled Grid-Connected DFIG Wind Turbine

Iker Oraa, Javier Samanes, Jesus Lopez and Eugenio Gubia
Electrical, Electronic and Communication Engineering
Institute of Smart Cities
Public University of Navarre (UPNA)
Pamplona, Spain
iker.oraa@unavarra.es

***Abstract*—The application of droop control techniques without inner current control loops to doubly-fed induction generator (DFIG) based wind turbines does not allow to provide a stable response at all operating points in terms of rotational speed and active and reactive power. After modeling the system dynamics and analyzing the causes of instability, this paper proposes a control strategy that allows to stabilize the system response at all possible operating points. Simulation results performed in MATLAB/Simulink validate the proposed control strategy proving its effectiveness.**

***Index Terms*—Doubly-fed Induction Generator (DFIG), Droop Control, Stability Analysis, Control strategy**

I. Introduction

Synchronous generators (SG) of conventional fossil-fuel power plants have been responsible for controlling the electric power system from its origin. However, in the near future, these generators are expected to be replaced by renewable energies (RREE) such as wind power, which is called to play a key role in this energy transition process towards a renewable-based generation system.

DFIG based wind turbines are the dominant technology in onshore wind farms [1]. As SGs are replaced by RREE, such as DFIG based wind farms, grid stability may be compromised, as grid-following (GFL) control strategies implemented in most power converters do not contribute to system stability. In recent years, research has focused on the development of grid-forming (GFM) control strategies that allow power converters to ensure a stable and safe operation of the power system [2]–[4]. GFM grid-connected power converters behave as voltage sources, imposing both the voltage amplitude and frequency and regulating the output active and reactive power. Among the existing GFM control strategies droop control has been widely studied [5], [6]. In droop-controlled grid-connected power converters two control loops are implemented, an active power-frequency droop control loop (P-ω) and a reactive power-voltage control loop (Q-V), which adjust the phase angle and amplitude of the voltage imposed by the converter, respectively.

Droop control has been mainly applied to grid-connected power converters and, although it has also been applied to DFIG wind turbines, there is not much work done so far in this regard. In almost all studies, in addition to droop control loops, inner current and/or voltage loops are implemented [7]–[11]. However, these inner control loops can be eliminated, what allows droop control to resemble the control of a SG [12]. In addition, with no inner loops the control structure is simpler, and the dynamic response and small-signal stability improve [13]. In [14] a droop control without inner control loops is implemented, and a small-signal model that accurately represents the system stability and dynamic response is proposed. In the same article, the proposed model shows that the conventional droop control applied to a DFIG turbine can not provide a stable response. As verified in this article, system dynamics is influenced by both the rotational speed and the active and reactive power level, and at certain operating points the system response is unstable.

To stabilize the response of droop-controlled DFIG wind turbines, it is necessary to modify the conventional droop control strategy to adapt it to the particularities of DFIG wind turbines. Therefore, in this paper, using the model proposed in [14], the causes of instability are analyzed and once understood, the solutions to stabilize the response and improve the dynamics are proposed, thus enabling the droop control without inner current loops of DFIG wind turbines and providing them with grid-forming characteristics. The proposed control solutions are validated in MATLAB/Simulink proving their effectiveness.

II. System Description and Stability Analysis

A. System Description

The system under study, illustrated in Fig. 1, represents a grid-connected DFIG wind turbine. The rotor-side converter (RSC) is directly connected to the rotor and controls the torque and rotational speed. The grid-side converter (GSC) controls its output current, i_{GSC}, to regulate the DC-bus voltage, v_{DC}, and it is connected to the stator terminals through the converter inductor, L_{GSC}. The GSC and RSC are connected through the DC-link capacitor, C_{DC}. The grid is modeled as an ideal voltage source with a series inductance, L_g. The voltage v_s represents the stator voltage, and the currents i_s, i_r, and i_g the stator, rotor, and grid currents, respectively.

This work was supported by the Spanish State Research Agency (AEI) under Grant PID2019-110956RB-I00/AEI/10.13039.

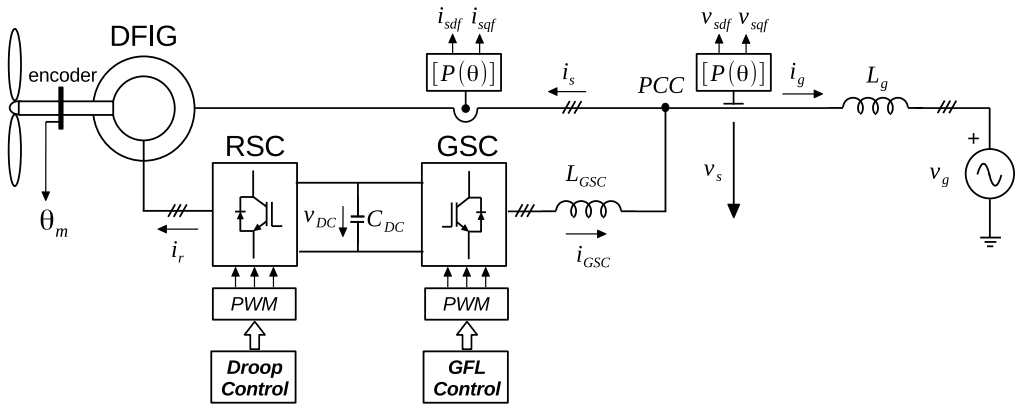

Fig. 1. System under study.

The system is controlled in the synchronous reference frame or dq axis. In the GSC a conventional GFL control is applied, while in the RSC a droop control, with no inner current and voltage control loops, is implemented. The droop control scheme is given in Fig. 2. On the one hand, the Q-V control loop adjusts the voltage amplitude imposed by the RSC. The PI controller provides an increase in the rotor voltage magnitude, ΔV_r, which is added to the rotor reference voltage, $V_{r,ref}$, obtaining the rotor reference voltage on the d axis, $V_{rd,ref}$. The q component of the rotor voltage reference is zero so that the rotor voltage is oriented along that d axis of the rotating dq reference frame. On the other hand, the P-ω control loop regulates the frequency and phase of the rotor voltage. The P-ω control loop provides a frequency increase, $\Delta\omega$, proportional to the difference between the reference active power, $P_{s,ref}$, and the measured active power, $P_{s,meas}$, and to the P-ω droop coefficient, m_p. The m_p coefficient represents the rate between the frequency deviation over nominal $\Delta f/f_n$ and the power increment over nominal $\Delta P/P_n$. This frequency increase is added to the reference frequency ω_{ref} (which is the grid nominal frequency) to obtain the dq axis rotational speed, ω. Then, through the integration of ω, the angle θ is obtained. This angle determines the position of the dq rotating axis over a stationary reference frame used for the application of Park transformation of the stator variables. The angle θ_r required for the application of Park transformation of the rotor variables depends on the position of the rotor, θ_m, that is measured by the DFIG shaft encoder. To obtain the instantaneous rotor voltages, $v_{r,ref}$, that will be modulated by the RSC, the inverse Park transformation, $[P^{-1}(\theta_r)]$, is applied. To calculate the stator active and reactive powers the filtered measurements of the stator voltages and currents in dq axis, v_{sdf}, v_{sqf}, i_{sdf} and i_{sqf}, are used.

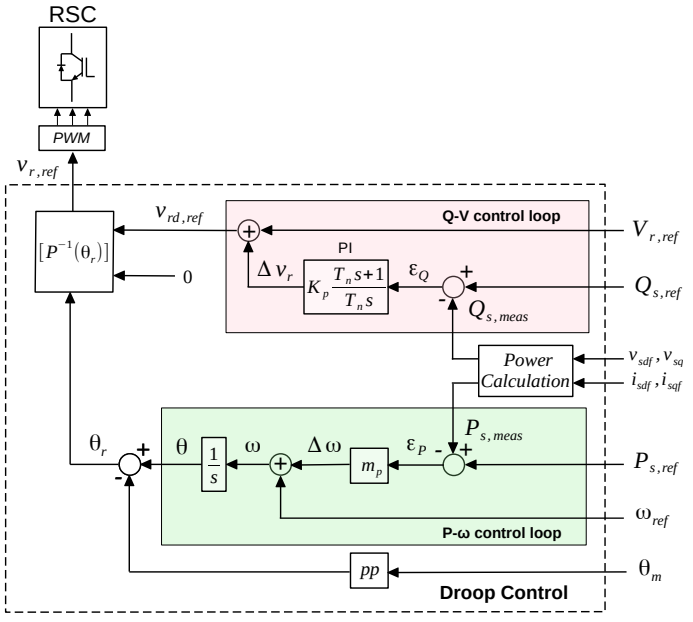

Fig. 2. Droop control scheme.

It should be noted that the GSC, due to the faster dynamics of the current control, has little influence on small-signal stability, so when analyzing system stability its analysis is neglected as in [15].

B. Stability Analysis

For the implementation of the droop control strategy represented in Fig. 2, a preliminary stability analysis is performed taking the system parameters summarized in Table I and using the small-signal model proposed in [14]. The model proposed in [14] is represented in block diagram form in Fig. 3. This model is based on the Park's vector approach and models the DFIG and its interaction with the control, accurately reproducing the system stability and dynamics. As shown in Fig. 3, the control adjusts the amplitude, ΔV_{rd}, frequency, $\Delta\omega$, and phase, $\Delta\theta$, of the rotor voltage according to the active and reactive power errors, ϵ_P and ϵ_Q. The plant (DFIG + Grid block) models the dynamics of the stator currents and voltages, ΔI_{sdq} and ΔV_{sdq}, which, after being filtered by an analog low-pass filter, $[LPAF(s)]$, are used to model the dynamics of stator active and reactive powers ([PQ] block).

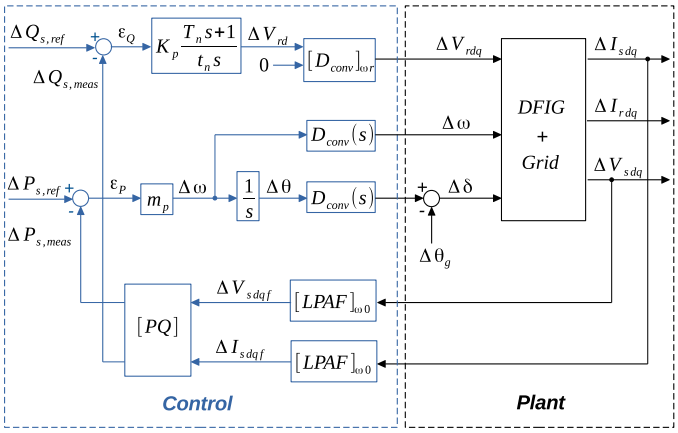

Fig. 3. Block diagram representation of the proposed model.

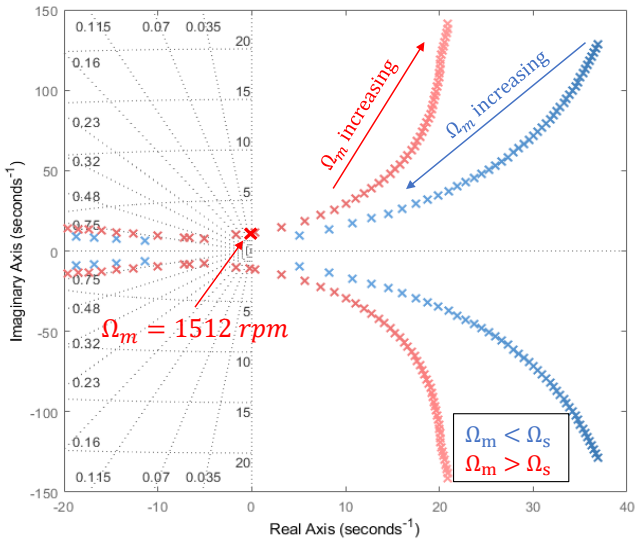

Fig. 4. Closed-loop pole variation for the whole range of possible rotational speeds.

Once the model has been implemented in MATLAB, the closed-loop poles of the system across the operating speed range of the machine have been obtained. The operation is limited to a $slip = \omega_r/\omega_0 = \pm 30\%$, where ω_0 is the grid nominal rotational speed and ω_r is the rotor electrical rotational speed defined as the difference between ω_0 and the mechanical rotational speed ω_m. Therefore, the operating speed ranges from 1050 to 1950 rpm, since the grid nominal frequency, f_0, is 50 Hz and the machine has two pole pairs. In Fig. 4, the evolution of the closed-loop poles as a function of the machine's rotational speed, Ω_m, is plotted. The poles corresponding to rotational speeds below the synchronous speed, Ω_s, are represented in blue, and the poles corresponding to speeds above the synchronous speed are shown in red. This way, the stability range of the system under study is determined. As can be seen in Fig. 4, the system is unstable over the whole operating speed range of the machine except from 1500 to 1512 rpm.

TABLE I
SYSTEM PARAMETERS (REFERRED TO THE STATOR)

Parameter	Magnitude
Grid $S_B = 2\ MVA,\ U = 690\ V,\ f_g = 50\ Hz$	
Line reactance (L_g)	0.1 p.u.
Line resistance (R_g)	0.015 p.u.
DFIG $S_B = 2\ MVA,\ U = 690\ V,\ f_{gen} = 50\ Hz$	
Rotor resistance (R_r)	0.0018 Ω
Rotor leakage inductance (L_{lr})	76.3 μH
Stator resistance (R_s)	0.0032 Ω
Stator leakage inductance (L_{ls})	161 μH
Mutual inductance (L_m)	0.0025 H
Pole pairs (pp)	2
Power converter	
Sampling frequency	5.7 kHz
Control parameters	
P-f droop coefficient (m_p)	0.05 p.u.
Q-V PI proportional gain (K_p)	$0.33 slip$ p.u.
Q-V PI integral time constant (T_n)	0.01
Cutoff frequency of low-pass analog filters (ω_c)	$2\pi 1500$ rad/s
References for simulations	
Active power initial reference at 1050 rpm ($P_{s,ref,0}$)	0 MW
Active power final reference at 1050 rpm ($P_{s,ref,f}$)	0.2 MW
Active power initial reference at 1470 rpm ($P_{s,ref,0}$)	0.8 MW
Active power final reference at 1470 rpm ($P_{s,ref,f}$)	1 MW
Reactive power reference ($Q_{s,ref}$)	0 MVA
Angular frequency (ω_{ref})	$2\pi 50$ rad/s
Voltage reference ($V_{r,ref}$)	$690 slip$ V

To analyze the causes of instability the MIMO GBC theory is applied [16]. According to this theory, the stability of any MIMO system, as the 2x2 dynamic model obtained for a DFIG wind turbine controlled in the synchronous reference frame, can be analyzed through the Bode diagram of the open-loop matrix eigenvalues. This criterion (MIMO GBC) stablishes that the number of closed-loop unstable poles, Z, is equal to the number of open-loop unstable poles, P, minus the total number of $\pm m180$ degrees crossings (m odd integer) with positive magnitude counted in the Bode diagram of all the system open-loop eigenvalues, C^+ (crossings with increasing phase), C^- (with decreasing phase) and C_0 (at 0 Hz)

$$Z = P + [2(C^+ - C^-) + C_0]. \quad (1)$$

The open-loop matrix eigenvalues, that correlate output active and reactive powers, $P_{s,meas}$ and $Q_{s,meas}$, with power errors, ϵ_P and ϵ_Q, are represented in Fig. 5 for rotational speeds of 1050 and 1470 rpm. Thanks to the frequency-domain analysis of the eigenvalues, two causes of instability are identified.

On the one hand, as can be observed in Fig. 5 (a), at 1050 rpm, there are two poorly damped poles at 15 Hz. This frequency coincides with the rotor electrical frequency, f_r. As previously mentioned, the grid nominal frequency, f_0, is 50 Hz and at 1050 rpm the $slip = 0.3$ so the rotor electrical frequency, $f_r = slip f_0$, is 15 Hz. However, it should be noted that this frequency is referred to dq reference frame and corresponds to an inverse sequence, that is, the frequency is -15 Hz. Therefore, in a stationary reference frame with the

stator, $\alpha\beta_s$, these two poorly damped poles would be seen at 35 Hz since $f_{\alpha\beta_s} = f_{dq} + f_0$ where $f_{\alpha\beta_s}$ is the frequency in $\alpha\beta_s$ and f_{dq} is the frequency in dq. This frequency coincides with the rotor mechanical frequency, f_m. If the frequency of the rotor voltage seen from a stationary reference frame is equal to the rotor mechanical frequency, 35 Hz in this case, it means that the rotor windings see a DC voltage, and therefore the impedance of the machine is minimum. Consequently, the rotor current is maximum, and the stator active power is also maximum. Due to this pair of poles, there is a -180 degree crossing with positive magnitude and decreasing phase (C^- = 1), marked by the orange dot, in the phase diagram of the eigenvalue λ_2. So as the system has no open-loop unstable poles (P = 0), according to (1) the closed-loop system has 2 unstable poles, Z = 2.

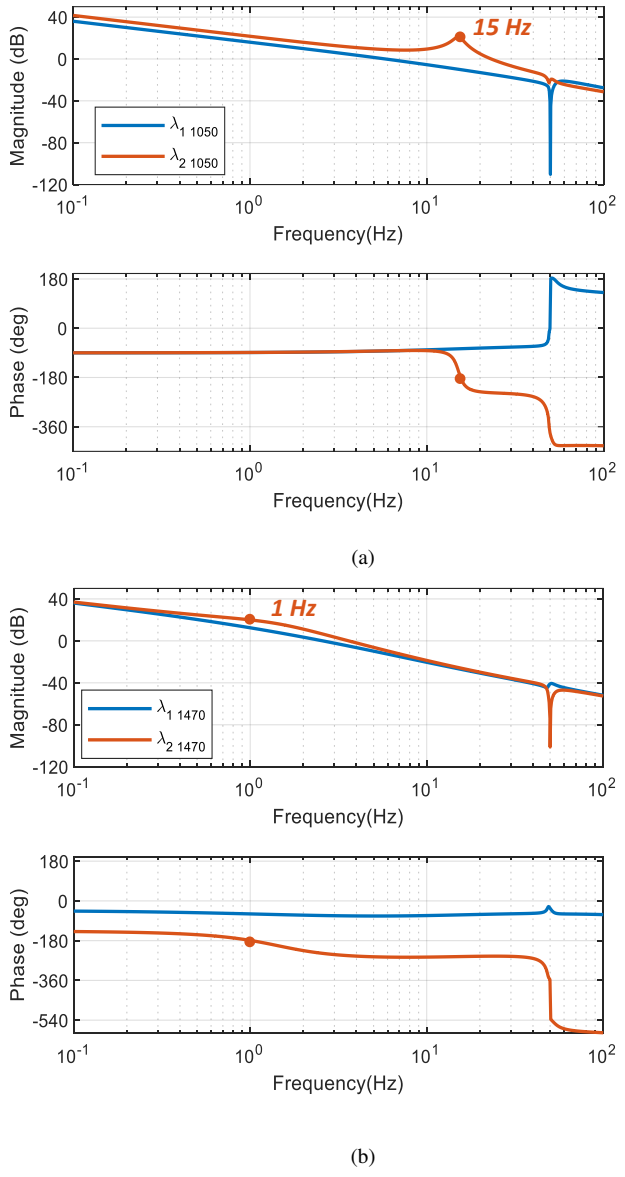

Fig. 5. Eigenvalues' Bode diagram: (a) at Ω_m=1050 rpm, and (b) at Ω_m=1470 rpm

On the other hand, as can be seen in Fig. 5 (b), at 1470 rpm, these poles are damped, but the -180 degree crossing with positive magnitude and decreasing phase (C^- = 1), marked by the orange dot, still occurs due to the phase loss of the eigenvalue λ_2, at low frequencies, and consequently, the closed-loop system still has 2 unstable poles, Z = 2. Near synchronism, that is, at low slips the rotor electrical frequency is very low, almost a DC component, and therefore the leakage reactance value drops and the machine shows a more resistive behavior (phase closer to 0 or ± 180 degrees, in this case closer to -180 degrees).

This way, it is concluded that the instability is produced by two causes; on the one hand, due to the low DC impedance at rotational speeds far from synchronism, that is, at high slips, and, on the other hand, due to the phase loss at low slips. Therefore, it becomes evident that the conventional droop control strategy must be modified to be applied to DFIG wind turbines. The next section presents the proposed control strategy.

III. Proposed Droop Control Strategy

As shown in the previous section, there are two causes of instability; a low DC impedance at high slips, and a phase decrease at low slips. In order to implement a conventional droop control without inner current loops in a DFIG wind turbine, two control solutions, depicted in red color in Fig. 6, are proposed; on the one hand, the emulation of a virtual resistor that increase the DC impedance solving the first cause of instability and, on the other hand, a rotation that increase the phase solving the second cause of instability.

A. Virtual Resistor Emulation

At high slips, as observed at 1050 rpm in Fig. 5 (a), there are two poorly damped poles at the electrical frequency of the rotor that destabilize the system. As mentioned, at this frequency the impedance of the machine is minimum so a solution to damp these poles is to increase the resistance value. For this purpose, the control can be adapted to emulate a virtual resistor [17].

The overall idea is to adjust the RSC voltage with respect to the current. As depicted in red color in Fig. 6, the RSC voltage reference is modified with respect to the stator current measurements proportionally to the virtual resistor, $[R_v]$. The addition of this virtual resistor would introduce a change of the voltage reference in steady state. To deal with this issue, a high-pass filter, $HPF(s)$, is added. The cutoff frequency of this high-pass filter is set one decade below the electrical frequency of the rotor, $\omega_{c,HPF}$=$|\omega_r|$/10. Therefore, the cutoff frequency of the filter will be variable, and, this way, the virtual resistor will act in the frequency range where the two poorly damped poles cause the instability.

As can be seen in Fig. 7 (a), introducing a virtual resistor at 1050 rpm, the poles causing instability are damped avoiding the -180 degree crossing with positive magnitude, and thus the system is stabilized.

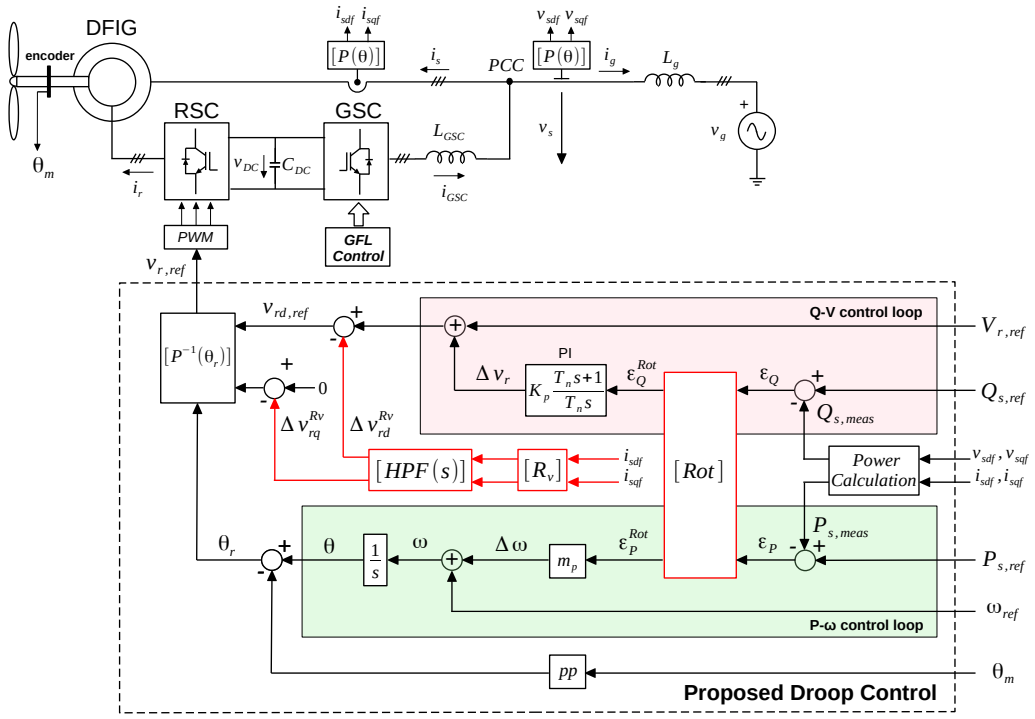

Fig. 6. Proposed droop control strategy for a DFIG wind turbine.

B. Phase Rotation

At low slips, as observed at 1470 rpm, these poles are already damped, and, as can be seen in Fig. 7 (b) (continuous lines), the virtual resistor does not allow to stabilize the system. There is a -180 degree crossing with positive magnitude at low frequency that introduces 2 unstable closed-loop poles. Nevertheless, the crossing appears in the eigenvalue λ_2, while the eigenvalue λ_1 has a sufficiently high phase margin. Consequently, if a rotation is introduced in the open-loop transfer matrix without changing the magnitude plot, the phase of the eigenvalue λ_2 can be increased and this -180 degree crossing can be avoided [18]. To modify the phase of the open-loop matrix eigenvalues, as shown in red color in Fig. 6, a rotation matrix, $[Rot]$, with a rotation angle α_R, is applied to power errors,

$$\begin{pmatrix} \epsilon_P^{Rot} \\ \epsilon_Q^{Rot} \end{pmatrix} = \begin{bmatrix} cos(\alpha_R) & -sin(\alpha_R) \\ sin(\alpha_R) & cos(\alpha_R) \end{bmatrix} \begin{pmatrix} \epsilon_P \\ \epsilon_Q \end{pmatrix}. \quad (2)$$

As can be seen in Fig. 7 (b) (dashed lines), adding a 90 degree rotation at 1470 rpm, the phase of the eigenvalue λ_2 increases avoiding the -180 degree crossing and stabilizing the system.

C. Adjustment of the control optimal parameters

Once it has been demonstrated that the combination of both control solutions, the virtual resistor and the phase rotation, allows stabilizing the system response at different operating speeds of the machine, for each operating point the value of these control parameters must be adjusted. For this purpose, an optimization process has been carried out. The objective of this optimization process is to minimize the root mean square error (RMSE) in the active and reactive power time response of the system in order to obtain a fast and damped time response. In other words, the active and reactive power response is optimized. The objective function is defined in (3).

$$f_{obj} = min(RMSE_P + RMSE_Q), \quad (3)$$

where

$$RMSE_P = \sqrt{\sum_{k=1}^{N}(P_s(k) - P_{s,ref}(k))^2/N}), \quad (4)$$

$$RMSE_Q = \sqrt{\sum_{k=1}^{N}(Q_s(k) - Q_{s,ref}(k))^2/N}), \quad (5)$$

where $(P_s(k) - P_{s,ref}(k))$ and $(Q_s(k) - Q_{s,ref}(k))$ are the deviations of the active and reactive power time response at the sample k and N is the sample size.

Thus, for each rotational speed and for each active and reactive power, the optimum virtual resistance and phase rotation values, that allow getting a fast and damped time response, have been obtained. In Fig. 8 the evolution of the closed-loop poles as a function of the machine's rotational speed, Ω_m, is plotted again, and as can be seen now, the system is stable over the whole operating speed range of the machine.

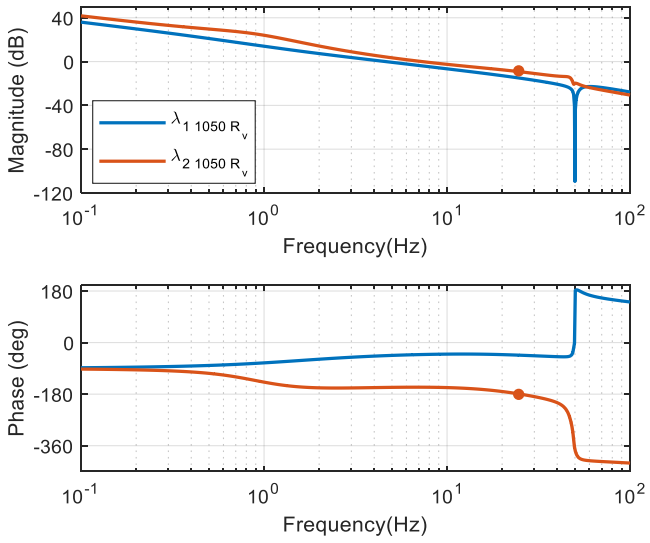

(a)

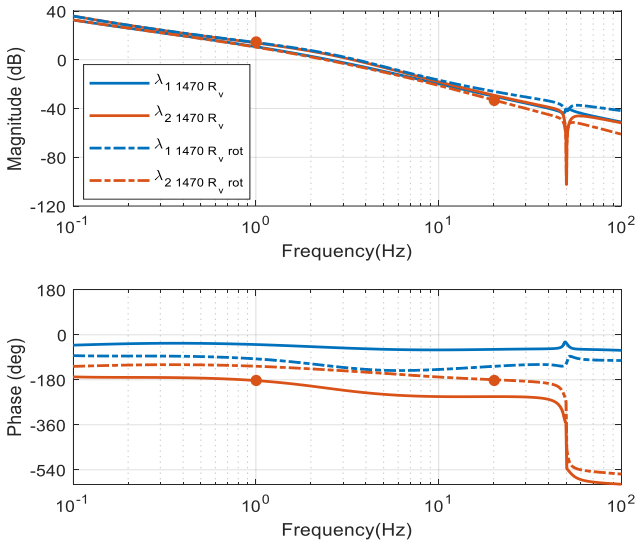

(b)

Fig. 7. Eigenvalues' Bode diagram: (a) at Ω_m=1050 rpm with a R_v = 0.5 pu, and (b) at Ω_m=1470 rpm with a R_v = 0.5 pu and a 90 degree rotation

IV. Simulation Results

To validate the proposed control solutions, a model is created in MATLAB/Simulink using the *Simscape Electrical Library*. The system parameters are the ones specified in Table. I.

Fig. 9 shows the active power evolution at 1050 rpm, Fig. 9 (a), and at 1470 rpm, Fig. 9 (b), as the proposed control solutions are transiently disabled. At 1050 rpm, at the beginning of the simulation, 4 s, with the virtual resistor enabled, a step from 0 MW to 0.2 MW is introduced in the reference active power, and the system response is stable, but when the R_v, is disabled at 5 s, the system becomes unstable. However, if the R_v is enabled at 5.1 s the system becomes stable again. This agrees with the stability analysis performed and shown in Fig. 5 (a) and Fig. 7 (a). Similarly, at 1470 rpm, with the virtual resistor and the phase rotation enabled, a step from 0.8 MW to 1 MW is introduced in the reference active power, and the system response is stable, as previously shown in Fig. 7 (b). However, when both the R_v and phase rotation are disabled at 5 s, the system becomes unstable. This agrees with the stability analysis performed in Fig. 5 (b). In any case, if the R_v and rotation are enabled at 5.1 s the system becomes stable again. These results confirm the stability analysis and the conclusions drawn from Fig. 5 and Fig. 7, and prove the effectiveness of the proposed control strategy.

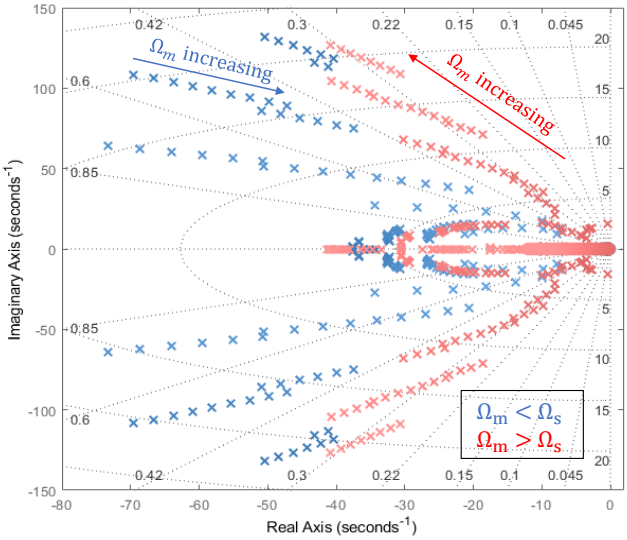

Fig. 8. Closed-loop pole variation for the whole range of possible rotational speeds with the proposed control strategy.

V. Conclusion

This paper analyzes the causes of instability of a DFIG wind turbine in which a droop-control without inner current and voltage control loops is implemented and proposes a control strategy to stabilize its response. Two causes of instability are identified; a low DC impedance at high slips, and a phase loss at low slips. In order to solve these instability problems, two control solutions are proposed; on the one hand, the emulation of a virtual resistor that increases the DC impedance solving the first cause of instability and, on the other hand, a rotation that increases the phase solving the second cause of instability. The combination of both control solutions allows not only to stabilize the system response over the whole range of rotational speeds and at all active and reactive power levels, but also, by optimizing its adjustment, the active and reactive power exhibit a fast and damped response.

Acknowledgment

The authors would like to thank Ingeteam Power Technology for its support.

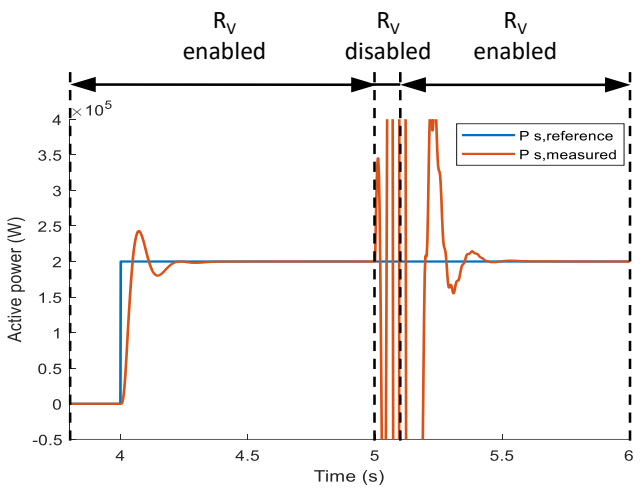

(a)

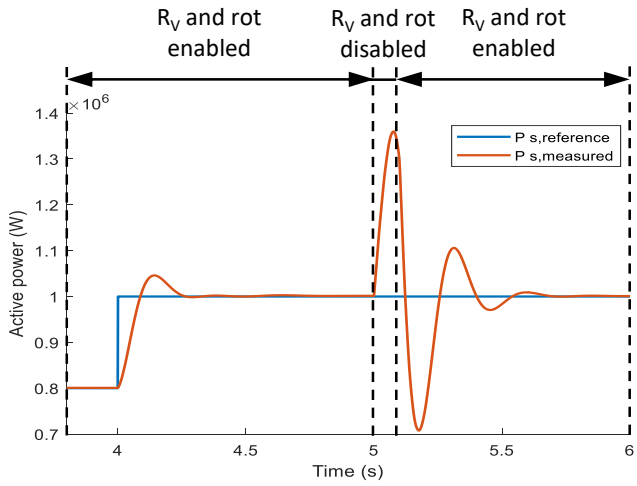

(b)

Fig. 9. Transient simulation disabling the proposed control solutions at 5 s: (a) at Ω_m=1050 rpm, and (b) at Ω_m=1470 rpm

REFERENCES

[1] T. Telsnig, "Wind energy technology development report 2020," 02 2021.

[2] R. Rosso, X. Wang, M. Liserre, X. Lu, and S. Engelken, "Grid-forming converters: Control approaches, grid-synchronization, and future trends—a review," *IEEE Open Journal of Industry Applications*, vol. 2, pp. 93–109, 2021.

[3] D. B. Rathnayake, M. Akrami, C. Phurailatpam, S. P. Me, S. Hadavi, G. Jayasinghe, S. Zabihi, and B. Bahrani, "Grid forming inverter modeling, control, and applications," *IEEE Access*, vol. 9, pp. 114 781–114 807, 2021.

[4] H. Zhang, W. Xiang, W. Lin, and J. Wen, "Grid forming converters in renewable energy sources dominated power grid: Control strategy, stability, application, and challenges," *Journal of Modern Power Systems and Clean Energy*, vol. 9, no. 6, pp. 1239–1256, 2021.

[5] J. M. Guerrero, J. C. Vasquez, J. Matas, L. G. de Vicuna, and M. Castilla, "Hierarchical control of droop-controlled ac and dc microgrids—a general approach toward standardization," *IEEE Transactions on Industrial Electronics*, vol. 58, no. 1, pp. 158–172, 2011.

[6] J. Rocabert, A. Luna, F. Blaabjerg, and P. Rodríguez, "Control of power converters in ac microgrids," *IEEE Transactions on Power Electronics*, vol. 27, no. 11, pp. 4734–4749, 2012.

[7] M. Marhaba, S. Farhangi, H. Imaneini, and R. Iravani, "Reactive power sharing improvement of droop-controlled dfig wind turbines in a microgrid," *IET Generation, Transmission & Distribution*, vol. 12, 10 2017.

[8] R. K. Rastogi and R. Sharma, "Improved synchronization and voltage regulation of dfig based wind energy system (wes)," in *2018 International Conference on Current Trends towards Converging Technologies (ICCTCT)*, 2018, pp. 1–5.

[9] Y. Han and J.-I. Ha, "Droop control using impedance of grid-integrated dfig within microgrid," *IEEE Transactions on Energy Conversion*, vol. 34, no. 1, pp. 88–97, 2019.

[10] H. Xiao, Z. Zhao, K. Zhou, J. Guo, C. S. Lai, and L. Lei Lai, "Voltage-source control of dfig in standalone wind power-based microgrids," in *2020 IEEE 1st China International Youth Conference on Electrical Engineering (CIYCEE)*, 2020, pp. 1–7.

[11] Z. Xie, X. Gao, S. Yang, and X. Zhang, "Improved fractional-order damping method for voltage-controlled dfig system under weak grid," *Journal of Modern Power Systems and Clean Energy*, pp. 1–10, 2021.

[12] T. Qoria, F. Gruson, F. Colas, G. Denis, T. Prevost, and X. Guillaud, "Inertia effect and load sharing capability of grid forming converters connected to a transmission grid," in *15th IET International Conference on AC and DC Power Transmission (ACDC 2019)*, 2019, pp. 1–6.

[13] W. Du, Z. Chen, K. P. Schneider, R. H. Lasseter, S. Pushpak Nandanoori, F. K. Tuffner, and S. Kundu, "A comparative study of two widely used grid-forming droop controls on microgrid small-signal stability," *IEEE Journal of Emerging and Selected Topics in Power Electronics*, vol. 8, no. 2, pp. 963–975, 2020.

[14] I. Oraa, J. Samanes, J. Lopez, and E. Gubia, "Modeling of a droop-controlled grid-connected dfig wind turbine," *IEEE Access*, vol. 10, pp. 6966–6977, 2022.

[15] Y. Jiao and H. Nian, "Grid-forming control for dfig based wind farms to enhance the stability of lcc-hvdc," *IEEE Access*, vol. 8, pp. 156 752–156 762, 2020.

[16] J. Samanes, A. Urtasun, E. L. Barrios, D. Lumbreras, J. López, E. Gubia, and P. Sanchis, "Control design and stability analysis of power converters: The mimo generalized bode criterion," *IEEE Journal of Emerging and Selected Topics in Power Electronics*, vol. 8, no. 2, pp. 1880–1893, 2020.

[17] T. Qoria, Q. Cossart, C. Li, X. Guillaud, F. Colas, F. Gruson, and X. Kestelyn, "Deliverable 3.2: Local control and simulation tools for large transmission systems," MIGRATE project, Report, 2018. [Online]. Available: https://www.h2020-migrate.eu/downloads.html

[18] J. Samanes, L. Rosado, E. Gubia, and J. Lopez, "Sub-synchronous resonance damper based on the stator voltage feedback for dfig wind turbines," in *2020 IEEE 21st Workshop on Control and Modeling for Power Electronics (COMPEL)*, 2020, pp. 1–8.